의공학회지 : 제18권, 제1호, 1997
J. of KOSOMBE : Vol. 18, No. 1

연 구 논 문
97-18-1-07

Optimal Velocity Profile for Minimum Power Consumption of Korean Total Artificial Heart

Jun Keun Chang, Ph.D. and, Byoung Goo Min, Ph.D.

= Abstract =

A dynamic model of the Korean total artificial heart(TAH) which contains a brushless DC motor, all of mechanical components, the pump system with integrated variable volume space(VVS) and the circulatory system model including the bronchial circulation were established. Two different sets of seven differential equations were separately derived for the left and right systolic period of the Korean TAH operation. Throughout the computer simulation, a full-state feedback optimal controller that minimizes the power consumption of the Korean TAH and drives the end stage velocity of the energy converter to zero was developed based upon the optimal control theory. Robustness of the controller were also analyzed with the dynamic model of the Korean TAH

Key words : Total artificial heart, Dynamic model, Full-state feedback optimal controller, Computer simulation

INTRODUCTION

The first successful use of the mechanical circulatory assistance device was reported in 1965[1]. Since that time, several applications of the various mechanical circulatory assist devices have been reported. Research and development of the total artificial heart (TAH) could be classified into the following three groups : the pneumatic TAH, the electrohydraulic TAH, and the electromechanical TAH[2]. The Korean TAH is one of the electromechanical TAHs and it converts electric power into the blood flow by the pendulous motion of a cylindrical actuator against a flexible blood sac[3].

To develop a totally implantable TAH, we adopted the "moving하ctuator" type energy converter with an integrated variable volume space(VVS) to eliminate the occupied space of the fixed하ctuator in the conventional electromechanical TAHs[3-6]. Throughout several trials of the anatomical fitting, it showed that the pumping chamber of the Korean TAH could be implanted inside the human thoracic cavity. But, the mass of the moving-actuator type energy converter was heavier than that of the conventional fixed-actuator type TAH, which generates large energy loss during the Korean TAH operation. Thus, the minimum power consumption of the implanted TAH is very important for the development of the transcutaneous energy transmission system and the internal battery for the orthotopic TAH system.

In this paper, the Bond-Graph modeling and the optimal control technique using the variational approach were used to develop a dynamic model of the Korean TAH and to simulate an optimal controller that minimizes the power consumption. In the dynamic model consisted of seven differential equations, a brushless DC motor, all of mechanical components, the pump system with integrated VVS and a simple circulatory

Institute of Biomedical Engineering Seoul National University
Department of Biomedical Engineering Seoul National University
통신저자 : Jun Keun Chang, Ph.D.
Institute of Biomedical Engineering Seoul National University 28 Yungun-dong, Chongno-gu, Seoul, 110-744, Korea
TEL : +82 (2) 740-8592, FAX : +82 (2) 3672-6950 E-mail : jkchang@bmews2.snu.ac.kr

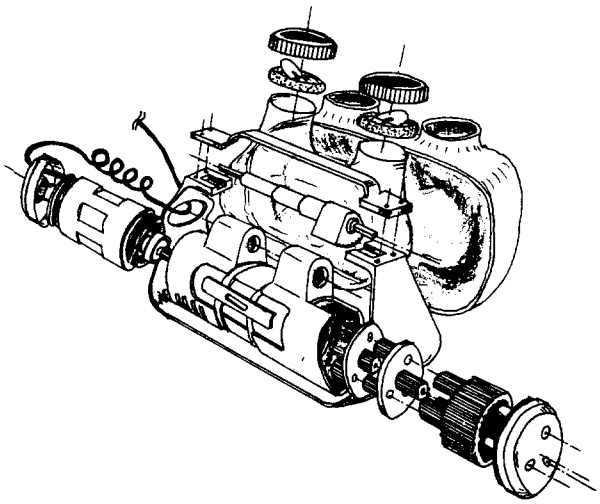

Fig. 1. Perspective view of the Korean TAH assembly

system model were included. Two different sets of seven differential equations were separately developed for the left and right systolic states of the Korean TAH. An optimal controller was developed with these dynamic models of the Korean TAH and the circulatory model. This controller drives the Korean TAH through a desired stroke angle while forcing the end stage velocity of the energy converter to zero. The value of the final time for the left and right systolic strokes was determined by the desired heart rate of TAH. Optimal control theory was used to find a velocity profile of the energy converter that minimizes the electric power consumption of the Korean TAH. To obtain the robustness of the controller, a closed loop control scheme was used.

MATERIALS AND METHODS

1. Mathematical Model of Artificial Heart

A brushless DC motor(Sierracin/Magnedyne 566-18) was is to drive the Korean TAH. The rotational movement of the motor' rotor is transferred to the planetary gear train of the energy converter of which total systemic gear ratio is 1/60. With high reduction of rotational movement, high torque is transferred to the 2nd torque-plate and the pinion of the last hypocyclic gear train. The pinion, which travels together with the energy converter, moves back and forth on the rack gear of the hypocyclic gear train

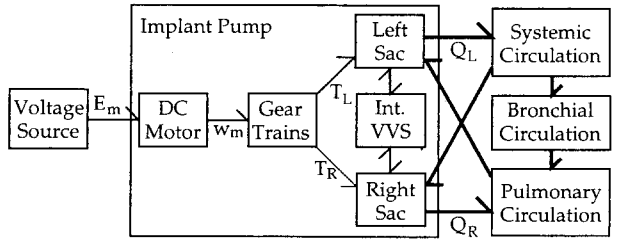

Fig. 2. System configuration of Korean TAH

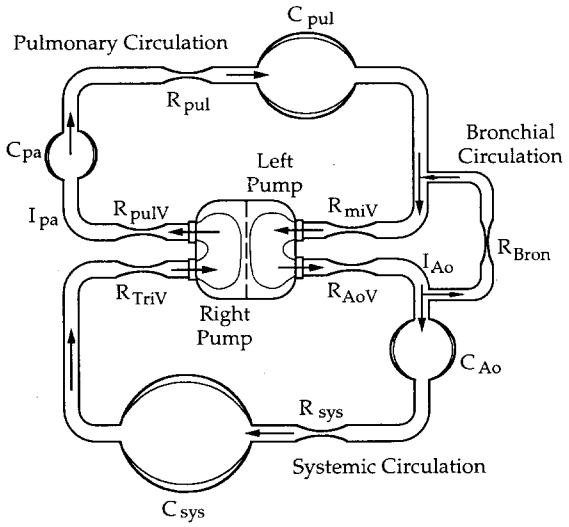

Fig. 3. Circulatory system model

[3]. Then the energy converter moves back and forth between two ventricles. For the lubrication and heat dissipation, the rest space inside the pump chamber is filled partially with the motor oil. Figure 1 shows the perspective view of the Korean TAH assembly.

The block diagram of the implanted Korean TAH that includes a brushless DC motor, gear trains including the journal bearings, two blood sacs and integrated VVS with a simple circulatory system is shown in Figure 2. In this circulatory system model, bronchial circulation was considered(Figure 3).

Mathematical models for the case of left blood sac only attached to the energy converter were derived for each left and right systolic period separately. Two Bond-Graphs of these models are shown in Figure 4 (a) and (b) for the left and right systolic period, respectively. Each of the Bond-Graphs was composed of several blocks : DC motor, energy converter, im-

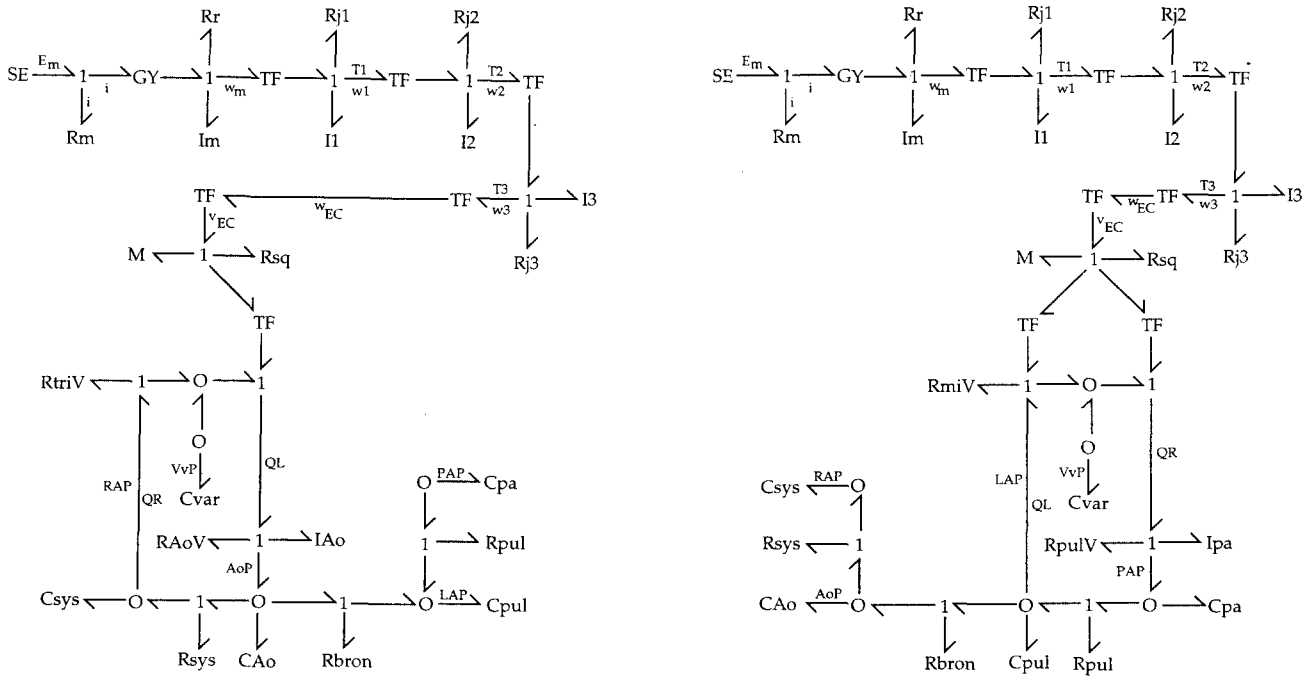

Fig. 4. The Bond-Graph of TAH : (a) left systolic period and (b) right systolic period

planted pump with VVS and the circulatory system.

Two algebraic equations were derived for DC motor. These equations were available for right systolic period if we change the sign of the rotation direction of the motor reversibly. The squeeze loss of motor oil between the rotor-stator gab was analyzed according to the hydrodynamic lubrication theory. Moments of inertia of the motor shaft and the 1st sun gear in the planetary gear train were added as a weighted value to that of the rotor. Inductance of the motor was neglected for the simplicity of the The governing equations of the energy converter were derived to analyze the torque and speed of each planetary gear train. The loss of journal bearing on each planetary gear train was evaluated with the hydrodynamic lubrication theory. Inertia losses of every planetary gear, gear shaft and cages were calculated. The governing equations for the energy converter are as follows :

$$i(t) = \frac{1}{R_m}\{e_m(t) - K_e \cdot \omega_m(t) \quad (1)$$

$$I_m \cdot \frac{\partial(\omega_m(t))}{\partial t} = K_i \cdot i(t) - R_r \cdot \omega_m(t) - T_m(t) \quad (2)$$

The governing equations of the energy converter were derived to analyze the torque and speed of each planetary gear train. The loss of journal bearing on each planetary gear train was evaluated with the hydrodynamic lubrication theory. Inertia losses of every planetary gear, gear shaft and cages were calculated. The governing equations for the energy converter are as follows :

$$T_m(t) = \frac{Gr_1}{eff_1}\left\{R_{j1} \cdot \omega_1(t) + I_1 \cdot \frac{\partial(\omega_1(t))}{\partial t} + T_1(t)\right\} \quad (3)$$

$$\omega_1(t) = Gr_1 \cdot \omega_m(t) \quad (4)$$

$$T_1(t) = \frac{Gr_2}{eff_2}\left\{R_{j2} \cdot \omega_2(t) + I_2 \cdot \frac{\partial(\omega_2(t))}{\partial t} + T_2(t)\right\} \quad (5)$$

$$\omega_2(t) = Gr_2 \cdot \omega_1(t) \quad (6)$$

$$T_2(t) = \frac{Gr_3}{eff_3}\left\{R_{j3} \cdot \omega_3(t) + I_3 \cdot \frac{\partial(\omega_3(t))}{\partial t} + T_3(t)\right\} \quad (7)$$

$$\omega_3(t) = Gr_3 \cdot \omega_2(t) \quad (8)$$

$$T_3(t) = \frac{Gr_{mf}}{eff_{mf}} \quad (9)$$

$$\omega_{EC}(t) = Gr_{mf} \cdot \omega_3(t) \quad (10)$$

Five equations were derived from the Bond-Graph in Figure 4-(a) for the left systolic period of pump operation. Squeeze of the motor oil during the reciprocating motion of the energy converter and the inertia loss of the moving energy converter were also considered according to the continuum theory. Since left blood sac only attached to energy converter for diastolic augmentation, right blood sac was assumed to move separately during left systolic period. In other words, the active ejection for the left blood sac and the passive filling for the right blood sac were guaranteed during the left systolic period. By the passive filling mechanism for right blood sacs, total amount of blood volume inflows from the right atrium was influenced by the pressure in integrated VVS as like equation (15). Thus, the governing equations for the pump with integrated VVS are as follows;

$$T_{EC}(t)=r\left\{R_{sq}\cdot V_{EC}(t)+M\cdot\frac{\partial(V_{EC}(t))}{\partial t}+F_{EC}(t)\right\} \tag{11}$$

$$V_{EC}(t)=r\cdot\omega_{EC}(t) \tag{12}$$

$$F_{EC}(t)=A_{pL}\left\{AoP(t)+R_{AoV}\cdot Q_L(t)+I_{Ao}\cdot\frac{\partial(Q_L(t))}{\partial t}-VvP(t)\right\} \tag{13}$$

$$Q_L(t)=A_{pL}\cdot V_{EC}(t) \tag{14}$$

$$C_{var}\cdot\frac{\partial(VvP(t))}{\partial t}=Q_R(t)-Q_L(t) \tag{15}$$

A modified Windkessel model with 5-elements was used and the bronchial circulation was also added to the model to simulate imbalance problem of the Korean TAH. About 10 % of left outflow was returned to the left blood sac by the bronchialation. The governing equations of the circulatory system are as follows :

$$C_{Ao}\cdot\frac{\partial(AoP(t))}{\partial t}=Q_L(t)-Q_{sys}(t)-Q_{Bronch}(t) \tag{16}$$

$$Q_{sys}(t)=\frac{AoP(t)-RAP(t)}{R_{sys}} \tag{17}$$

$$Q_{Bronch}(t)=\frac{AoP(t)-LAP(t)}{R_{Bronch}} \tag{18}$$

$$C_{sys}\cdot\frac{\partial(RAP(t))}{\partial t}=Q_{sys}(t)+Q_R(t) \tag{19}$$

$$Q_R(t)=\frac{RAP(t)-VvP(t)}{R_{TriV}} \tag{20}$$

$$C_{pul}\cdot\frac{\partial(LAP(t))}{\partial t}=Q_{pul}(t)+Q_{Bronch}(t) \tag{21}$$

$$Q_{pul}(t)=\frac{PAP(t)-LAP(t)}{R_{pul}} \tag{22}$$

$$C_{pa}\cdot\frac{\partial(PAP(t))}{\partial t}=-Q_{pul}(t) \tag{23}$$

By the summation of above equations from (1) to (23), the governing differential equations are derived as follows :

$$\begin{aligned}&\frac{\partial(\omega_{EC}(t))}{\partial t}\cdot\left\{\frac{I_m}{Gr_1\cdot Gr_2\cdot Gr_3\cdot Gr_{mf}}\right.\\&+\frac{Gr_1\cdot Gr_2\cdot Gr_3\cdot Gr_{mf}}{eff_1\cdot eff_2\cdot eff_3\cdot eff_{mf}}\cdot r^2(M+I_{Ao}\cdot A_{pL}^{\ 2})\\&+\frac{Gr_1}{eff_1}\cdot\frac{I_1}{Gr_2\cdot Gr_3\cdot Gr_{mf}}+\frac{Gr_1\cdot Gr_2}{eff_1\cdot eff_2}\cdot\frac{I_2}{Gr_3\cdot Gr_{mf}}\\&\left.+\frac{Gr_1\cdot Gr_2\cdot Gr_3}{eff_1\cdot eff_2\cdot eff_3}\cdot\frac{I_3}{Gr_{mf}}\right\}\\&=\omega_{EC}(t)\left\{-\frac{K_t\cdot K_e}{R_m\cdot Gr_1\cdot Gr_2\cdot Gr_3\cdot Gr_{mf}}\right.\\&-\frac{R_r}{Gr_1\cdot Gr_2\cdot Gr_3\cdot Gr_{mf}}-\frac{Gr_1\cdot Gr_2\cdot Gr_3\cdot Gr_{mf}}{eff_1\cdot eff_2\cdot eff_3\cdot eff_{mf}}\cdot\\&\cdot r^2\left(R_{sq}+R_{AoV}\cdot A_{pL}^{\ 2}\right)-\frac{Gr_1}{eff_1}\cdot\frac{R_{j1}}{Gr_1\cdot Gr_2\cdot Gr_3\cdot Gr_{mf}}\\&\left.-\frac{Gr_1\cdot Gr_2}{eff_1\cdot eff_2}\cdot\frac{R_{j2}}{Gr_3\cdot Gr_{mf}}-\frac{Gr_1\cdot Gr_2\cdot Gr_3}{eff_1\cdot eff_2\cdot eff_3}\cdot\frac{R_{j3}}{Gr_{mf}}\right\}\\&+\frac{K_t}{R_m}e_m(t)+\frac{Gr_1\cdot Gr_2\cdot Gr_3\cdot Gr_{mf}}{eff_1\cdot eff_2\cdot eff_3\cdot eff_{mf}}\cdot r\\&\cdot A_{pL}\{VvP(t)-AoP(t)\}\end{aligned} \tag{24}$$

$$\begin{aligned}&\frac{\partial(AoP(t))}{\partial t}=\frac{r\cdot A_{pL}}{C_{Ao}}\cdot\omega_{EC}(t)+\frac{LAP(t)}{R_{Bron}\cdot C_{Ao}}\\&-\left[\frac{1}{R_{sys}\cdot C_{Ao}}+\frac{1}{R_{Bron}\cdot C_{Ao}}\right]AoP(t)+\frac{RAP(t)}{R_{sys}\cdot C_{Ao}}\\&\frac{\partial(LAP(t))}{\partial t}=\frac{AoP(t)}{R_{Bron}\cdot C_{pul}}+\frac{PAP(t)}{R_{pul}\cdot C_{pul}}\end{aligned} \tag{25}$$

$$-\left[\frac{1}{R_{Br\,on}\cdot C_{pul}}+\frac{1}{R_{pul}\cdot C_{pul}}\right]LAP(t) \tag{26}$$

$$\frac{\partial(PAP(t))}{\partial t}=\frac{LAP(t)-PAP(t)}{R_{pul}\cdot C_{pa}} \tag{27}$$

$$\frac{\partial(RAP(t))}{\partial t}=\frac{AoP(t)}{R_{sys}\cdot C_{sys}}+\frac{VvP(t)}{R_{triV}\cdot C_{sys}}$$
$$-\left[\frac{1}{R_{sys}\cdot C_{sys}}+\frac{1}{R_{triV}\cdot C_{sys}}\right]RAP(t) \tag{28}$$

$$\frac{\partial(VvP(t))}{\partial t}=-\frac{r\cdot A_{pL}}{C_{var}}\cdot\omega_{EC}(t)$$
$$+\frac{RAP(t)-VvP(t)}{R_{triV}\cdot C_{var}} \tag{29}$$

Another seven equations were derived from the Bond-Graph in Figure 4-(b). Since the left blood sac was attached, the condition of active ejection and active filling were generated during the right systolic period. The contacting area between the left blood sac and the energy converter was larger than that of right as tested in the 3-cylinder model.

$$\frac{\partial(\omega_{EC}(t))}{\partial t}\cdot\left\{\frac{I_m}{Gr_1\cdot Gr_2\cdot Gr_3\cdot Gr_{mf}}\right.$$
$$+\frac{Gr_1\cdot Gr_2\cdot Gr_3\cdot Gr_{mf}}{eff_1\cdot eff_2\cdot eff_3\cdot eff_{mf}}\cdot r^2(M+I_{pa}\cdot A_{pR}{}^2)$$
$$+\frac{Gr_1}{eff_1}\cdot\frac{I_1}{Gr_2\cdot Gr_3\cdot Gr_{mf}}+\frac{Gr_1\cdot Gr_2}{eff_1\cdot eff_2}\cdot\frac{I_2}{Gr_3\cdot Gr_{mf}}$$
$$\left.+\frac{Gr_1\cdot Gr_2\cdot Gr_3}{eff_1\cdot eff_2\cdot eff_3}\cdot\frac{I_3}{Gr_{mf}}\right\}$$
$$=\omega_{EC}(t)\left\{-\frac{K_t\cdot K_e}{R_m\cdot Gr_1\cdot Gr_2\cdot Gr_3\cdot Gr_{mf}}\right.$$
$$-\frac{R_r}{Gr_1\cdot Gr_2\cdot Gr_3\cdot Gr_{mf}}-\frac{Gr_1\cdot Gr_2\cdot Gr_3\cdot Gr_{mf}}{eff_1\cdot eff_2\cdot eff_3\cdot eff_{mf}}$$
$$\cdot r^2\left(R_{sq}+R_{pul\,V}\cdot A_{pR}{}^2+R_{miV}\cdot A_{pL}{}^2\right)-\frac{Gr_1}{eff_1}$$
$$\cdot\frac{R_{j1}}{Gr_2\cdot Gr_3\cdot Gr_{mf}}-\frac{Gr_1\cdot Gr_2}{eff_1\cdot eff_2}\cdot\frac{R_{j2}}{Gr_3\cdot Gr_{mf}}$$
$$\left.-\frac{Gr_1\cdot Gr_2\cdot Gr_3}{eff_1\cdot eff_2\cdot eff_3}\cdot\frac{R_{j3}}{Gr_{mf}}\right\}+\frac{K_t}{R_m}e_m(t)$$
$$+\frac{Gr_1\cdot Gr_2\cdot Gr_3\cdot Gr_{mf}}{eff_1\cdot eff_2\cdot eff_3\cdot eff_{mf}}\cdot r$$
$$\cdot A_{pL}\{VvP(t)-LAP(t)\}+\frac{Gr_1\cdot Gr_2\cdot Gr_3\cdot Gr_{mf}}{eff_1\cdot eff_2\cdot eff_3\cdot eff_{mf}}\cdot r$$
$$\cdot A_{pR}\{PAP(t)-VvP(t)\} \tag{30}$$

$$\frac{\partial(AoP(t))}{\partial t}=\frac{LAP(t)}{R_{syy}}\cdot C_{Ao}+\frac{RAP(t)}{R_{sys}\cdot C_{Ao}}$$
$$-\left[\frac{1}{R_{sys}\cdot C_{Ao}}+\frac{1}{R_{Br\,on}\cdot C_{Ao}}\right]AoP(t) \tag{31}$$

$$\frac{\partial(LAP(t))}{\partial t}=\frac{r\cdot A_{pL}}{C_{pul}}\cdot\omega_{EC}(t)+\frac{AoP(t)}{R_{Br\,on}\cdot C_{pul}}$$
$$+\frac{PAP(t)}{R_{pul}\cdot C_{pul}}-\left[\frac{1}{R_{Br\,on}\cdot C_{pul}}+\frac{1}{R_{pul}\cdot C_{pul}}\right]LAP(t) \tag{32}$$

$$\frac{\partial(PAP(t))}{\partial t}=\frac{LAP(t)-PAP(t)}{R_{pul}\cdot C_{pa}}-\frac{r\cdot A_{pR}}{C_{pa}}\cdot\omega_{EC}(t) \tag{33}$$

$$\frac{\partial(RAP(t))}{\partial t}=\frac{AoP(t)-RAP(t)}{R_{sys}\cdot C_{sys}} \tag{34}$$

$$\frac{\partial(VvP(t))}{\partial t}=\frac{r\cdot(A_{pL}-A_{pR})}{C_{var}\cdot\omega_{EC}}(t) \tag{35}$$

$$\frac{\partial(VvP(t))}{\partial t}=-\frac{r\cdot A_{pL}}{C_{var}}\cdot\omega_{EC}(t)$$
$$-\frac{RAP(t)-VvP(t)}{R_{triV}\cdot C_{var}} \tag{36}$$

2. Formulation of Optimal Control Problem

The optimal controller was designed to drive the Korean TAH through a desired stoke angle while minimizing the electrical power consumption, and forcing the end stage velocity of its energy converter to zero. Minimum power consumption was very important to reduce the size and the weight of the internal battery and zero end-stage velocity would give more comfortable condition to the recipient[7-9].

Recasting Equation (24)-(35) in the standard form with the state vector $X(t)$ and input $U(t)$ as fol-

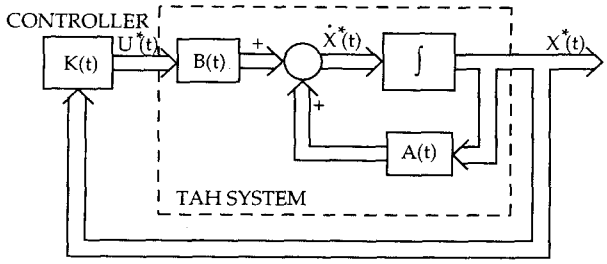

Fig. 5. The structure of the optimal feedback control system

lows :

$$X(t)=[\theta_{EC}(t)\ \omega_{EC}(t)\ AoP(t)\ PAP(t)\ RAP(t)\ VvP(t)]^T \quad (37)$$

$$U(t)=e_m(t) \quad (38)$$

The stroke angle of the energy converter was added to the system variables for its control. Thus, the system state equations for left systolic period is as follows :

$$\frac{\partial(X(t))}{\partial t}=A_L\cdot X(t)+B_L\cdot U(t) \quad (39)$$

where

$$A_{L1,2}=1$$

$$A_{L2,2}=\frac{\alpha_L}{\beta_L}$$

$$A_{L2,3}=\frac{\frac{Gr_1\cdot Gr_2\cdot Gr_3\cdot Gr_{mf}}{eff_1\cdot eff_2\cdot eff_3\cdot eff_{mf}}r\cdot A_{pL}}{\beta_L}$$

$$A_{L2,7}=\frac{\frac{Gr_1\cdot Gr_2\cdot Gr_3\cdot Gr_{mf}}{eff_1\cdot eff_2\cdot eff_3\cdot eff_{mf}}r\cdot A_{pL}}{\beta_L}$$

$$A_{L3,2}=\frac{r\cdot A_{pL}}{C_{Ao}}$$

$$A_{L3,3}=-\frac{1}{C_{Ao}}\cdot\frac{R_{Brom}+R_{sys}}{R_{Brom}\cdot R_{sys}}$$

$$A_{L3,4}=-\frac{1}{R_{Brom}\cdot C_{Ao}}$$

$$A_{L5,3}=-\frac{1}{R_{sys}\cdot C_{Ao}}$$

$$A_{L4,3}=-\frac{1}{R_{Brom}\cdot C_{pul}}$$

$$A_{L4,4}=-\frac{1}{C_{pul}}\cdot\frac{R_{Brom}+R_{pul}}{R_{Brom}\cdot R_{pul}}$$

$$A_{L4,5}=-\frac{1}{R_{pul}\cdot C_{pul}}$$

$$A_{L5,4}=-\frac{1}{R_{pul}\cdot C_{pa}}$$

$$A_{L5,5}=-\frac{1}{R_{pul}\cdot C_{pa}}$$

$$A_{L6,3}=-\frac{1}{R_{sys}\cdot C_{sys}}$$

$$A_{L6,6}=-\frac{1}{C_{sys}}\cdot\frac{R_{triV}+R_{sys}}{R_{triV}\cdot R_{sys}}$$

$$A_{L6,7}=-\frac{1}{R_{triV}\cdot C_{sys}}$$

$$A_{L7,2}=-\frac{r\cdot A_{pL}}{C_{var}}$$

$$A_{L7,6}=-\frac{1}{R_{triV}\cdot C_{var}}$$

$$A_{L7,7}=-\frac{1}{R_{triV}\cdot C_{var}}$$

other components of A_L are zero. (40)

$$\alpha_L=-\frac{K_t\cdot K_e}{R_m\cdot Gr_1\cdot Gr_2\cdot Gr_3\cdot Gr_{mf}}-\frac{R_r}{Gr_1\cdot Gr_2\cdot Gr_3\cdot Gr_{mf}}$$
$$-\frac{Gr_1\cdot Gr_2\cdot Gr_3\cdot Gr_{mf}}{eff_1\cdot eff_2\cdot eff_3\cdot eff_{mf}}\cdot r^2\left(R_{sq}+R_{AoV}\cdot A_{pL}^2\right)$$
$$-\frac{Gr_1}{eff_1}\cdot\frac{R_{j1}}{Gr_2\cdot Gr_3\cdot Gr_{mf}}-\frac{Gr_1\cdot Gr_2}{eff_1\cdot eff_2}\cdot\frac{R_{j2}}{Gr_3\cdot Gr_{mf}}$$
$$-\frac{Gr_1\cdot Gr_2\cdot Gr_3}{eff_1\cdot eff_2\cdot eff_3}\cdot\frac{R_{j3}}{Gr_{mf}} \quad (41)$$

$$\beta_L = \frac{I_m}{Gr_1 \cdot Gr_2 \cdot Gr_3 \cdot Gr_{mf}} + \frac{Gr_1 \cdot Gr_2 \cdot Gr_3 \cdot Gr_{mf}}{eff_1 \cdot eff_2 \cdot eff_3 \cdot eff_{mf}} \cdot r^2 \left(M + I_{Ao} \cdot A_{PL}^{\ 2} \right) + \frac{Gr_1}{eff_1} \cdot \frac{I_1}{Gr_2 \cdot Gr_3 \cdot Gr_{mf}} + \frac{Gr_1 \cdot Gr_2}{eff_1 \cdot eff_2} \cdot \frac{I_2}{Gr_3 \cdot Gr_{mf}} + \frac{Gr_1 \cdot Gr_2 \cdot Gr_3}{eff_1 \cdot eff_2 \cdot eff_3} \cdot \frac{I_3}{Gr_{mf}} \quad (42)$$

$$B_L = \begin{bmatrix} 0 & \frac{K_t}{\beta_L \cdot R_m} & 0 & 0 & 0 & 0 & 0 \end{bmatrix}^T \quad (43)$$

and the similar state equations for the right systolic period could be derived with the same method.

The instantaneous power consumption w(t) could be represented as follows :

$$w(t) = e_m(t) \cdot i(t) \quad (44)$$

The motor current could be obtained as a function of the energy converter angular velocity and the motor input voltage. Thus, total energy consumption during a one stroke could be derived as follows :

$$J(t) = \int_{t_0}^{t_f} w(t)\, dt \quad (45)$$

where $t_0$and t_f are the initial and final time of the stroke, respectively. Equation (44) indicates that the power consumption is a function of the motor input voltage, energy converter's angular velocity, and system parameters dependent on the mechanical components.

Minimum power consumption could be achieved by optimizing the hardware design and the optimal input profile of the motor voltage. The optimal input voltage and the velocity profile for specific system parameters are obtained through the numerical approach. Then, the design optimization of system parameters could be simulated easily with the simple change of them. Thus, the problem could be restated as a general optimal control problem as follows :

Minimize the cost junction J

$$J(t) = \int_{t_0}^{t_f} \left(X^T NU + \frac{1}{2} U^T RU \right) dt \quad (46)$$

so that

$$J(t) = \int_{t_0}^{t_f} \left\{ \frac{e_m^{\ 2}(t)}{R_m} - \frac{K_e}{R_m \cdot Gr^1 \cdot Gr^2 \cdot Gr^3 \cdot Gr^{mf}} \omega_{EC}(t) \cdot e_m(t) \right\} dt \quad (47)$$

where

$$N = \begin{bmatrix} 0 & -\frac{K_e}{R_m \cdot Gr_1 \cdot Gr_2 \cdot Gr_3 \cdot Gr_{mf}} & 0 & 0 & 0 & 0 \end{bmatrix}^T \quad (48)$$

$$R = \frac{2}{R_m} \quad (49)$$

The boundary conditions for the left systolic period are as follows :

$$X(t_0) = [0 \;\; 0 \;\; AoP_i \;\; LAP_i \;\; PAP_i \;\; RAP_i \;\; VvP_i]^T \quad (50)$$

$$X(t_f) = [\theta_d \;\; 0 \;\; free \;\; free \;\; free \;\; free \;\; free]^T \quad (51)$$

and for the right systolic period are :

$$X(t_0) = X(t_f) \mid_{left\ systole} \quad (52)$$

$$X(t_f) = [0 \;\; 0 \;\; free \;\; free \;\; free \;\; free \;\; free]^T \quad (53)$$

3. Formulation of Optimal Feedback Control

The closed-loop controller was used for compensating the errors of control signals due to the uncertainties of the system parameters. Full state feedback optimal regulator was implemented as a closed loop optimal controller. Figure 5 shows the structure of the optimal feedback control system.

The two-point boundary value optimal control problem could be recasted as the free end conditions optimal control problem by adding the penalty term to the cost function :

$$\frac{1}{2} X'(t_f)^T \cdot H \cdot X'(t_f) \quad (54)$$

and the new state vector $X'(t)$ defined as follows :

$$X'(t)=[\theta_{EC}(t)-\theta_d \quad \omega_{EC}(t) \quad AoP(t) \quad LAP(t) \quad PAP(t) \quad RAP(t) \quad VvP(t)]^T \tag{55}$$

where θ_d was the desired final stroke angle of the energy converter. The cost function could be recasted as follows :

$$J(t)=\frac{1}{2}X'(t_f)^T\cdot H\cdot X'(t_f)+\int_{t_0}^{t_f}\left\{X'(t_f)^T NU(t)+\frac{1}{2}U(t)^T RU(t)\right\}dt \tag{56}$$

where H is the weighing matrix that was a trade-off between the power consumption and the accuracy of the final conditions. Increasing H will decrease the deviations of the end conditions at the expense of increasing power consumption, and vice versa.

$$H=\begin{bmatrix} h_1 & 0 & 0 & 0 & 0 & 0 & 0 \\ 0 & h_2 & 0 & 0 & 0 & 0 & 0 \\ 0 & 0 & 0 & 0 & 0 & 0 & 0 \\ 0 & 0 & 0 & 0 & 0 & 0 & 0 \\ 0 & 0 & 0 & 0 & 0 & 0 & 0 \\ 0 & 0 & 0 & 0 & 0 & 0 & 0 \\ 0 & 0 & 0 & 0 & 0 & 0 & 0 \end{bmatrix} \tag{57}$$

Because θ_d was a constant value for each stroke, the system equation (38) could be rewritten as follows :

$$\frac{\partial(X'(t))}{\partial t}=A_L\cdot X(t)+B_L\cdot U(t) \tag{58}$$

In addition, the first column of matrix A was zero, the new system equation could be expressed as follows :

$$\frac{\partial(X'(t))}{\partial t}=A_L\cdot X'(t)+B_L\cdot U'(t) \tag{59}$$

with the new initial condition for left systolic period :

$$X'(t_0)=[-\theta_d \quad 0 \quad AoP_i \quad LAP_i \quad PAP_i \quad RAP_i \quad VvP_i]^T \tag{60}$$

and for right systolic period :

$$X'(t_0)=[\theta_d \quad 0 \quad AoP_{f\_left} \quad LAP_{f\_left} \quad PAP_{f\_left} \quad RAP_{f\_left} \quad VvP_{f\_left}]^T \tag{61}$$

Calculus of variations technique was used to solve the above two-point boundary value problems. Applying the Pontryagin's minimum principle to the above problem, the Hamiltonian could be obtained as follows :

$$H[X'(t),\ U'(t),\ p'(t),\ t]=X'(t)^T NU'(t)+\frac{1}{2}U'(t)^T RU'(t)+p'(t)^T\{A\cdot X'(t)+B\cdot U'(t)\} \tag{62}$$

where $p'(t)$ was the costate vector.

Optimal control $U'(t)$ could be obtained under the following conditions to minimize the power consumption of the energy converter :

For all $t\in[t_0,\ t_f]$

$$\text{State equation : } \frac{\partial X'(t)^*}{\partial t}=A\cdot X(t)^*+B\cdot U'(t)^* \tag{63}$$

$$\text{Costate equation : } \frac{\partial X'(t)^*}{\partial t}=-\frac{\partial H}{\partial X'}=-N\cdot U'(t)-A^T\cdot p'(t)^* \tag{64}$$

$$\text{Control equation : } \frac{\partial H}{\partial U'}=N^T\cdot X'(t)^*+R\cdot U'(t)^*+B^T\cdot p'(t)^*=0 \tag{65}$$

Thus, optimal control $U'(t)$ of equation (64) was expressed as follows :

$$U'(t)^*=-R^{-1}[N^T\cdot X'(t)^*+B^T\cdot p'(t)^* \tag{66}$$

Substituting equation (65) into (62) and (63), optimal state equation and costate equation were expressed in standard matrix form :

$$\begin{bmatrix} \frac{\partial}{\partial t}(X'(t)^*) \\ \frac{\partial}{\partial t}(p'(t)^*) \end{bmatrix}=\begin{bmatrix} (A-B\cdot R^{-1}\cdot N^T & -B\cdot R^{-1}\cdot B^T \\ N\cdot R^{-1}\cdot N^T & (N\cdot R^{-1}\cdot B^T-A^T \end{bmatrix}\begin{bmatrix} X'(t)^* \\ p'(t)^* \end{bmatrix} \tag{67}$$

The solution of this matrix equation has the form with partitioned transition matrix $\Phi(t_f,\ t)$:

$$\begin{bmatrix} \frac{\partial}{\partial t}(X'(t)^*) \\ \frac{\partial}{\partial t}(p'(t)^*) \end{bmatrix}=\begin{bmatrix} \Phi_{11}(t_f,\ t) & \Phi_{12}(t_f,\ t) \\ \Phi_{12}(t_f,\ t) & \Phi_{22}(t_f,\ t) \end{bmatrix}\cdot\begin{bmatrix} X'(t)^* \\ p'(t)^* \end{bmatrix} \tag{68}$$

Using the calculus of variations, the transversality condition was obtained of the free end conditions :

$$p'(t_f)^* = H \cdot X'(t_f)^* \tag{69}$$

with substituting equation (68) into (67), the optimal costate vector obtained as follows :

$$p'(t_f)^* = [\Phi_{22}(t_f, t) - H \cdot \Phi_{12}(t_f, t)]^{-1} \cdot [H \cdot \Phi_{11}(t_f, t) - \Phi_{21}(t_f, t)] \cdot X'(t_f)^* \tag{70}$$

or in the form :

$$p'(t_f)^* = K(t) \cdot X'(t_f)^* \tag{71}$$

where

$$K(t) = [\Phi_{22}(t_f, t) - H \cdot \Phi_{12}(t_f, t)]^{-1} \cdot [H \cdot \Phi_{11}(t_f, t) - \Phi_{21}(t_f, t)] \tag{72}$$

It could be shown that the matrix $K(t)$ satisfies the matrix Riccati equation :

$$\frac{\partial}{\partial t}K(t) = -K(t)[A - BR^{-1}N^T] + [NR^{-1}B^T - A^T]K(t) + NR^{-1}N^T + K(t)BR^{-1}B^TK(t) \tag{73}$$

with the initial condition :

$$K(t_f) = H \tag{74}$$

Actually, $K(t)$ depend on t_f, and t_f must be specified.

Substituting equation (70) and (72) into equation (65), optimal control could be derived as follows :

$$U'(t)^* = F(t) \cdot X'(t)^* \tag{75}$$

where $F(t)$ was the feedback gain matrix of optimal regulator controller.

$$F(t) = -R^{-1}[N^T + B^T \cdot K(t)] \tag{76}$$

At last, the optimal state trajectories were calculated from the system equation (57) :

$$\frac{\partial}{\partial t}X'(t)^* = [A + B \cdot F(t)]X'(t)^* \tag{77}$$

In addition, the matrix Riccati equation (72) was independent of the system state value that enables one to calculate it off-line.

4. Numerical Simulation

Numerical simulations for the closed loop optimal controller were performed. Discrete numerical simulations were executed on the IBM PC with FORTRAN 77.

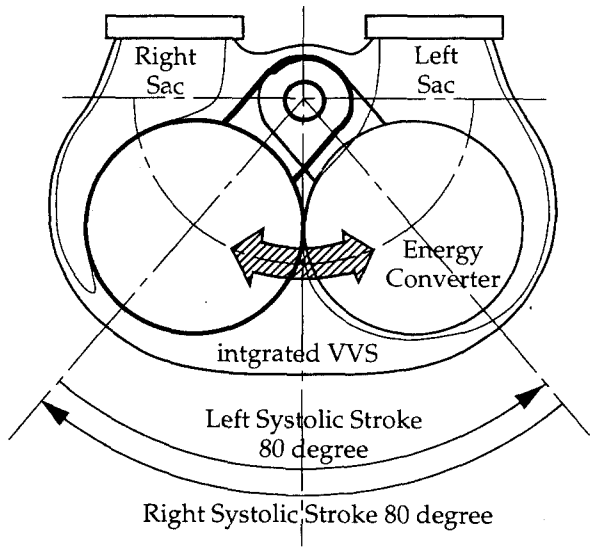

Fig. 6. Schematic diagram of simulation operation

To solve the matrix Riccati equation, Runge-Kutta 4th order method with the adaptive step size control was implemented. Since Riccati gain matrix $K(t)$ was symmetric, the system of 28 ordinary differential equations could be solved simultaneously. The heart rate was fixed with 60 beat/minute during the simulation, and the time interval $(t_f - t_0)$ was 0.5 sec. The Riccati gain matrix was independent of the state initial condition values, Riccati gain vector could be calculated off-line, which was attractive in the real time control applications. Finite difference method was applied to the calculation of the optimal state trajectory with 0.5 msec sampling time.

RESULTS

1. Effect of Weighting Matrix H on Optimal Control

Desired final stroke angle is 80 degree. The left systolic stroke condition was simulated first, and then, the right systolic stroke was performed successively. Simulation scheme is shown in Figure 6. To analyze the effect of weighting matrix H, two different H matrix were tested for the left systolic period. To approve the less than 1 degree deviation of the

final position, larger H was needed for the left systolic period.

$$H=\begin{bmatrix} 5 & 0 & 0 & 0 & 0 & 0 & 0 \\ 0 & 10 & 0 & 0 & 0 & 0 & 0 \\ 0 & 0 & 0 & 0 & 0 & 0 & 0 \\ 0 & 0 & 0 & 0 & 0 & 0 & 0 \\ 0 & 0 & 0 & 0 & 0 & 0 & 0 \\ 0 & 0 & 0 & 0 & 0 & 0 & 0 \\ 0 & 0 & 0 & 0 & 0 & 0 & 0 \end{bmatrix} \quad (78)$$

$$H=\begin{bmatrix} 50 & 0 & 0 & 0 & 0 & 0 & 0 \\ 0 & 100 & 0 & 0 & 0 & 0 & 0 \\ 0 & 0 & 0 & 0 & 0 & 0 & 0 \\ 0 & 0 & 0 & 0 & 0 & 0 & 0 \\ 0 & 0 & 0 & 0 & 0 & 0 & 0 \\ 0 & 0 & 0 & 0 & 0 & 0 & 0 \\ 0 & 0 & 0 & 0 & 0 & 0 & 0 \end{bmatrix} \quad (79)$$

Substituting the parameter values listed in Table 1 [10], the system equations were resulted as follows :

$$\frac{\partial}{\partial t}X(t)=\begin{bmatrix} 0 & 0 & 0 & 0 & 0 \\ 0 & -157.8 & -4.611 & 0 & 0 \\ 0 & 6.383 & -0.827 & 0.075 & 0 \\ 0 & 0 & 0.1 & -10.1 & 10 \\ 0 & 0 & 0 & 10 & -10 \\ 0 & 0 & 0.206 & 0 & 0 \\ 0 & -36.69 & 0 & 0 & 0 \end{bmatrix}$$

$$\begin{bmatrix} 0 & 0 \\ 0 & 4.611 \\ 0.752 & 0 \\ 0 & 0 \\ 0 & 0 \\ -8.797 & 8.591 \\ 180 & -180 \end{bmatrix} X(t)+\begin{bmatrix} 0 \\ 71.97 \\ 0 \\ 0 \\ 0 \\ 0 \\ 0 \end{bmatrix} e_m(t) \quad (80)$$

with initial state value for left systolic stroke :

$$X_0=[-80 \quad 0 \quad 90 \quad 5 \quad 30 \quad 15 \quad 0]^T \quad (81)$$

and the time interval $t_0=0.0$ and $t_f=0.5$. N and R matrices for the cost function were as follows :

$$N=[0 \quad -1.089 \quad 0 \quad 0 \quad 0 \quad 0 \quad 0]^T \quad (82)$$

$$R=1.0101 \quad (83)$$

The results of the numerical simulation are presented from Figure 7 to Figure 11. Figure 8 shows the optimal controller gain for the 1st state variable, the stroke angle of the energy converter, and 2nd state variable, the angular velocity of the energy converter, with different H, respectively. Figure 9 represents the stroke angle of the energy converter with the optimal controller. For the large afterload of the systemic circulation, the larger H value is needed during the left systolic period. The optimal velocity pro-

Table 1. Values of modeling parameters of the Korean TAH

R_m	1.98	[ohms]
R_r	2.956	[kg-mm²/s]
I_m	0.6398	[kg-mm²]
K_e	0.036	[V-s/rad]
K_t	36238.75	[kg-mm²/s²-A]
Gr_1	0.2143	
Gr_2	0.2143	
Gr_3	0.2727	
Gr_{mf}	1.3333	
eff_1	0.9724	
eff_2	0.9724	
eff_3	0.9724	
eff_m	0.986	
I_1	1.148	[kg-mm²]
I_2	1.5466	[kg-mm²]
I_3	6.822	[kg-mm²]
Rj_1	0.0382	[kg-mm²/s]
Rj_2	0.121	[kg-mm²/s]
Rj_3	1.086	[kg-mm²/s]
r	28	[mm]
M	0.478	[kg]
R_{sq}	0.3853	[kg/s]
A_{pL}	2274	[mm²]
A_{pR}	1891	[mm²]
C_{var}	231.385	[mm³/mmHg]
C_{Ao}	1330	[mm³/mmHg]
C_{pa}	1000	[mm³/mmHg]
C_{pul}	1000	[mm³/mmHg]
C_{sys}	4850	[mm³/mmHg]
I_{Ao}	2.753×10^6	[kg/mm⁴]
I_{pa}	2.7×10^7	[kg/mm⁴]
R_{AoV}	5.0×10^5	[mmHg-s/mm³]
R_{Bron}	0.01	[mmHg-s/mm³]
R_{miV}	2.4×10^5	[mmHg-s/mm³]
R_{pul}	1.0×10^4	[mmHg-s/mm³]
R_{pulV}	3.0×10^5	[mmHg-s/mm³]
R_{sys}	0.001	[mmHg-s/mm³]
R_{triV}	2.4×10^5	[mmHg-s/mm³]

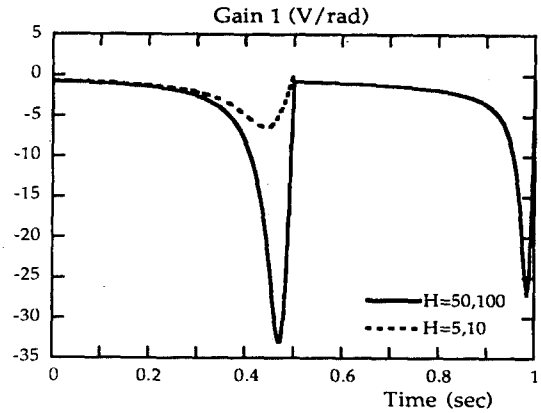

Fig. 7. Simulation of 1st controller gain with different H

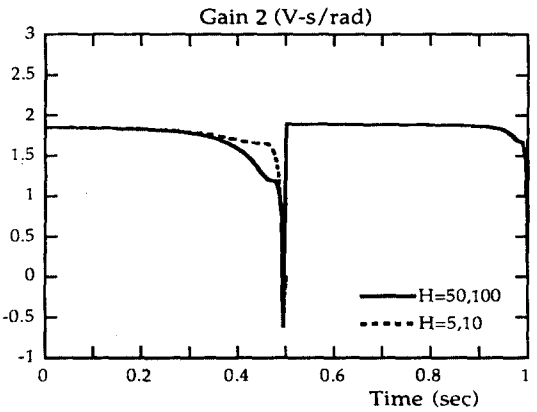

Fig. 8. Simulation of 2nd controller gain with different H

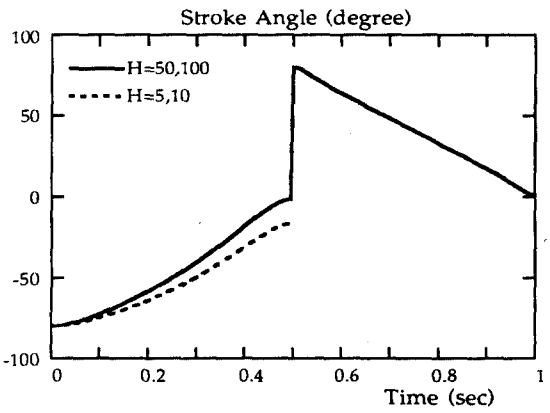

Fig. 9. Simulation of stroke angle with different H

files and the power consumption with different H are shown in Figure 10 and Figure 11, respectively.

2. Optimal Velocity Profiles for Minimum Power Consumption

The acquired optimal velocity profile was compared

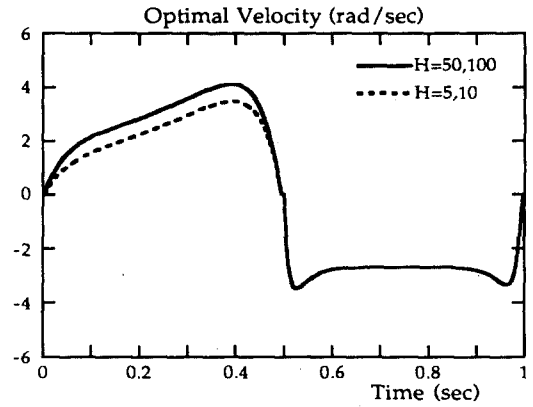

Fig. 10. Simulation of optimal velocity profile with different H

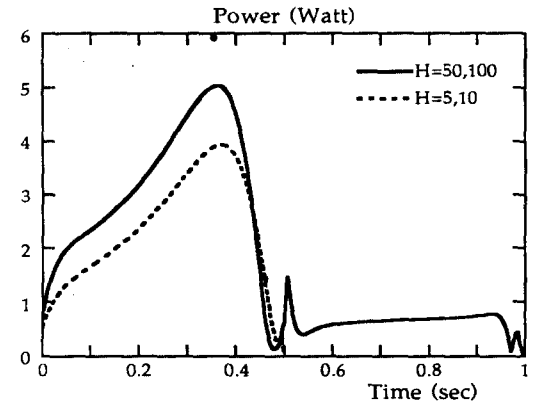

Fig. 11. Simulation of power consumption with different H

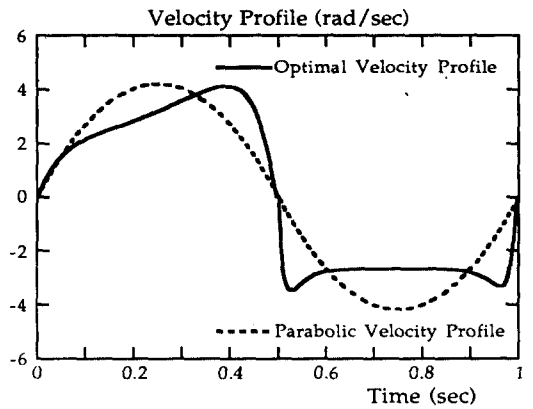

Fig. 12. Comparison of velocity profiles

with the parabolic velocity profiles currently used. Comparison of the energy consumption between the parabolic velocity profile and the new optimal velocity profile is shown in Table 2. Comparison of motor cur-

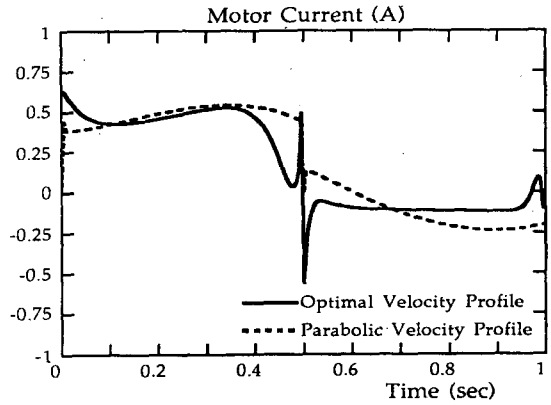

Fig. 13. Comparison of motor currents

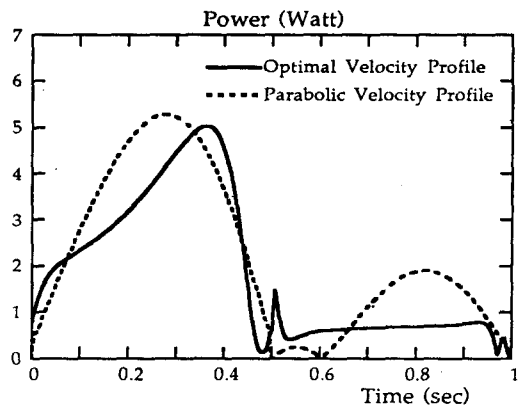

Fig. 14. Comparison of power consumption

Table 2. Comparison of energy consumption between parabolic velocity profile and the optimal velocity profile

Simulation Mode	Energy Consumption(Joules)		Reduction of Energy (%)
	Parabolic	Optimal Profile	
Left Systolic Period	1.720	1.501	12.7
Right Systolic Period	0.483	0.313	35.2

rent and power consumption between the parabolic velocity profile and the optimal velocity profile are shown in Figure 13 and Figure 14, respectively.

DISCUSSION

A dynamic model of the Korean TAH was developed and elucidated with the computer simulation. In this dynamic model that was consisted of seven differential equations, a brushless DC motor, all of mechanical components, the pump system with integrated VVS and a simple circulatory system model with the bronchial circulation were included. Two different sets of seven differential equations were separately developed for the left and right systolic periods of the Korean TAH operation.

To minimize the power consumption of the Korean TAH, the optimal controller with the mathematical model of the Korean TAH and the circulatory model has been developed. The optimal controller minimizes the Korean TAH's power consumption, and drives the end stage velocity of the energy converter to zero. To obtain the robustness of the controller, a closed loop controller was developed. Optimal velocity profile and optimal voltage input profile were also calculated for each conditions. The optimal gains can be precalculated by off-line. It can be implemented optimally for any initial states. Comparisons in the energy consumption between the parabolic velocity profile and the optimal velocity profile control were simulated. 12.7%-35.2% of energy consumption was saved with the optimal velocity profile compared to that of the parabolic velocity profiles.

The gain of the optimal controller was calculated using the lumped parameter model, and values of parameters were listed in Table 1. However, the systemic resistance varies as 0.0007mmHg/mm^3-sec to 0.00136 mmHg/mm^3-sec in the vascular system. The parameter sensitivity had been investigated through simulations. It had been simulated for different systemic resistance using the optimal feedback gains calculated for the systemic resistance of 0.001mmHg/mm^3-sec. The robustness of controller was summarized in Table 3. It was also shown that the increased power consumption was negligible. Consequently, the optimal controller was seemed to be robust to variations in systemic resistance.

In conclusion, from the numerical simulation of the dynamic models, the performance of the Korean TAH can be predicted without in vitro and in vivo experiments. This study shows that the dynamic model of the Korean TAH, the minimum power consumption controller, and the numerical simulation could be very feasible for the design and development of TAH[11]. Computer simulation based on the dynamic model is

Table 3. Controller robustness with respect to systemic resistance

	Left Systolic Period			Right Systolic Period		
R_{sys} for Gain Calc. (mmHg/mm³-sec)	0.001	0.001	0.001	0.001	0.001	0.001
R_{sys} (mmHg/mm³-sec)	0.001	0.0007	0.0013	0.001	0.0007	0.0013
Stroke Angle (degree)	79.2	79.4	78.9	79.0	79.1	78.9
Peak Power (Watt)	5.03	4.92	5.22	0.77	0.78	0.76
Energy (Joules)	1.501	1.462	1.578	0.313	0.317	0.308

also expected to be usefully applied to develop the automatic control algorithm of TAH.

REFERENCES

1. F. C. Spencer, U. G. Eiseman, at al., "*Assisted circulation for cardiac failure following intracardiac surgery with cardiopulmonary bypass*", Journal of Thoracic Cardiovascular Surgery, 46, 135, 1965
2. Kazuhiko Atsumi, "*Research and development on the total artificial heart-from the engineering aspects*", Artificial Organs, 10(1), 12-19, 1986
3. Byoung G. Min, Jun K. Chang, et al., "*A tether-free, moving actuator total artificial heart*", Transaction of American Society of Artificial Internal Organs, XXXVI, 249-251, 1990
4. William J. Weiss, William S. Pierce, et al., "*Permanent circulatory support systems at the Pennsylvania state university*", IEEE Transaction on Biomedical Engineering, 37(2), 138-144, 1990
5. Robert T. Kung, Param I. Singh, et al., "*A unique left-right flow imbalance compensation scheme for an implantable total artificial heart*", Transaction of American Society of Artificial Internal Organs, XXXV, 486-488, 1989
6. Takeshi Izutsu, Yukihiko Nose, et al., "*Methods for volume assessment of an air filled compliance chamber*", Transaction of American Society of Artificial Internal Organs, XXXV, 481-483, 1989
7. Uri Tasch, H. K. Hsu, et al., "*A novel feedback pusher plate controller for the Penn state electric ventricular assist device*", Journal of Dynamic Systems, Measurement and Control, 111, 69-74, 1989
8. M. Keith Sharp and Don B. Olsen, "*Sensitivity of the artificial heart to changes in vascular resistance*", Transaction of American Society of Artificial Internal Organs, XXXVI, 805-810, 1990
9. Uri Tasch, David B. Geselowitz, et al., "*An adaptive aortic pressure observer for the Penn state electric ventricular assist device*", IEEE Transaction on Biomedical Engineering, 37(4), 374-383, 1990
10. Jun Keun Chang, "*Simulation of dynamic models & optimal control for Korean total artificial heart*", Master thesis, Seoul National University, 1992
11. Alexander Y. Lerner, "*Artificial blood circulation: stabilization, physiological control, and optimization*", Artificial Organs, 14(2), 110-117, 1990

=국문초록=

브러쉬없는 직류전동기, 작동기내의 모든 기계요소, 가변체적공간과 혈액펌프, 기관지순환을 고려한 혈액순환계를 포함하는 한국형 완전 인공심장의 동역학적 모델을 개발하였다. 좌심실 수축기와 우심실 수축기에 대해서 각각 일곱개의 미분방정식을 유도하였으며, 최적제어이론을 이용하여 인공심장의 에너지 소모를 최소화하는 최적제어기를 설계하였다. 컴퓨터 수치해석을 통해서 한국형 인공심장의 동작을 분석하였으며, 제안된 최적제어기의 강인성을 해석하였다.